Supplementary materials

Romain Dupuis[a,b,c], **Pierre-Louis Valdenaire (the late)**[c], **Roland J.-M. Pellenq**[c,d], **and Katerina Ioannidou**[b,c]

[a]IEM and ICGM, Univ. Montpellier, CNRS, Montpellier, France; [b]LMGC, Univ. Montpellier, CNRS, Montpellier, France; [c] MIT/CNRS/Aix-Marseille Université Joint Laboratory "MultiScale Materials Science for Energy and Environment", UMI MSE2 , Massachusetts Institute of Technology, 77 Massachusetts Avenue, Cambridge, Massachusetts 02139, USA; [d]International Research Laboratory, EPIDAPO, CNRS-George Washington U., Washington DC

A. Review of the models for ionic adsorption. Activated carbons (typically activated with high concentration of KOH or steamed water at high temperature) is a special class of amorphous nanoporous carbons that have been intensively used as supercapacitor electrode materials by controlling the resulting nanoporosity, pore size distribution and surface chemistry (functional oxygen-containing groups, (1)). Hence, the texture parameters at the nanoscale can be tuned to optimize the electrochemical performance of supercapacitors. Nanostructured electrodes have gained increasing popularity as the manipulation of nanoporosity and surface functional groups leads to an enhancement in the gravimetric capacitance in supercapacitors, hence increasing the energy and power densities of carbon materials. The crucial relationship between the electrode structure and the applied potentials would grant the application of wider potential limits in aqueous systems and therefore achieving better supercapacitor electrochemical performance in terms of energy and power delivery.

The activation process of nanoporous carbons originally derived from the pyrolysis of some organic precussors such as saccharose, cellulose, etc) induces an increase in the overall porosity of the material by the removal of molecular size fragments weakly attached to the main carbon backbone that is essentially made of a percolative backbone of sp2 carbons (these sp2 carbon ensure electronic conductivity of the material due to weakly localized electrons). As a consequence, the activation process is known to lower electronic conductivity as it populates pore surface with oxygen-containing groups (that localize electrons) but also improves sub-nanopores connectivity. This latter characteristic was shown from Hybrid-Reverse-Monte-Carlo simulations of the 3D texture of non-activated (with a density of around 1.5 g/cc) and activated porous carbons (with a density of 1 g/cc) (1). This was recently further confirmed from out-of-equilibrium MD simulations of the flow of hydrocarbons (2).

Abouelamaiem et al. (3) studied cellulose-derived/KOH activated nanoporous carbons with different surface chemistry and porous textures using polarized in-situ Raman spectroscopy to obtain information on the structural changes of the activated carbons under strong electrochemical oxidation and reduction conditions. Raman data were shown to be correlated to the cyclic voltammograms obtained in high anodic and cathodic potentialsm conditions. The influence of the specific surface area, nanoporosity and oxygen-containing functional groups in the carbon substrate in supercapacitor applications was revealed: the conductivity, hence electrochemical performances of the KOH-activated carboneous electrodes was shown to be directly related to the oxygen content (docked in oxygen-containing functional groups at the pores surface, the largest the oxygen content, the lower the conductivity) but also to the total pore volume and the pore size distribution. Electrochemical Impedance Spectroscopy (EIS) allows the evaluation of the electronic charge transfer resistance in the carbon solid texture and electrolyte movement resistance under an applied ac potential. EIS is a non-destructive technique that has been applied to study porous electrode/electrolyte interfaces (4). EIS is one of the very few techniques that is sensitive to material porosity in particular it allows addressing the role sub-nanopores in porous carbons in polarized anodic or cathodic conditions when docking ions (5). Beguin et al. (6), Chmiola et al. (7) and Segalini et al. (8) previously demonstrated that electrodes with sub-nanopores can exhibit high specific capacitance, and attributed this phenomenon to distortion/removal of the ion's solvation sheath as it enters the charging pore; access to these sub-nanopores was strongly voltage dependent. That is, at low electrode voltages ions can be excluded from subnanopores, but at higher voltages, the ion solvation sheath can distort and rupture making naked ion docking possible. Thus, for a porous carbon having a given pore-size distribution starting from the subnano-range, one can expect that the strong potential-dependence reflects on its impedance. More specifically, we might expect an increase in measured storage pore capacitance and a decrease in resistance associated with ion storage in subnanopores. Suss et al. (5) indicated that high-frequency semi-circle type features have been observed for metal/electrolyte interfaces in the impedance Nquist plot (i.e. imaginary part of measured impedance plotted as a function of its real part) can be attributed to electrochemical redox reactions at the metallic/electrolyte interface although porous carbon electrodes are typically not associated with such so-called Faradaic pseudocapacitive-type ion storage mechanisms. This correlates well with the findings of Abouelamaiem et al who showed porous carbons do not reveal a clear Nquist semicircular plot, indicating insignificant charge transfer resistances due to redox reactions on functional pores surface groups above a certain potential threshold.

However, the non-ideality of nanoporous carbon surfaces, makes fundamental understanding of the electrochemical processes occurring very challenging as because of topological defects (compared to graphene plane hexagonal atomic arrangement) combined with chemical defects (functional oxygen-containing group non-sp2 carbon atoms (that are nevertheless forming a percolative backbone of the porous carbon matrix allowing for electronic conductivity. Very recently, Evlashin et al. (9) have shown that the including heteroatoms (O and N defects) into a graphene does lead to a substantial increase of the capacitance. In particular, they identified carbon lacunes as favorable sites for these chemical defects through partial oxidation of the carbon lattice. Hartmann and Hwang (10) applied computational methods to evaluate the energetics of the reduction (hydrogenation) and oxidation (hydroxylation) reactions on pristine graphene and showed local distortion of the carbon arrangement upon chemisorption of H and O

impurities upon polarization. Along the same line, Hussain et al (11) showed using quantum DFT that nanoporous defective graphene (NPG) can be used as an anode material for Li+, Na+, K+, Mg2+, and Ca2+-ion docking. They calculated structural properties, defect formation energies, metal binding energies, charge analysis, and electronic structures properties. In particular, they showed that upon substitution with oxygen-rich functional groups (e.g., O, OH, and COOH) and doping with heteroatoms (B, N, P, and S), the ion binding ability of NPG is significantly enhanced. Using nonequilibrium Green's function theory in Tight Binding (TB) and Density Functional Theory (DFT) schemes, G. Lee et al calculated the density of state of defective oxidized graphene and showed electron localization that upon substantial amounts of defects, is responsible for the inferior electronic transport quality than pristine graphene. Focusing on atomic partial charge distribution in graphene flakes, Maslechko et al. (12) showed that only pure sp2 carbons (i.e carbons connected to 3 other carbon atoms with an angle of 120 degree between them have a zero atomic partial charge while all others (carbon atoms connected to other elements such as H, O, N, B) do localize charge excess or deficit (depending on the polarization achieved by injecting or removing one electron). The unified picture that emerges from the above listed theoretical works on graphene is that defects of whatever form (chemical heterogeneity, H, O, N etc...) or topological (carbon atoms departing from the pure 6 C members ring in the sp2 state of wave function hybridization) are the locations of charge accumulation or deficit upon charge injection/removal mimicking voltage polarization and drive ion adsorption.

Based on the lessons from defective graphene and moving more specifically to nanoporous ordered carbons (replica from zeolites casting with pores size of 1 nm(13) and disordered activated carbons (1), Delfour (14) (in French) (15) calculated the electronic structure of these carboneous substrates using a TB (with a 2nd moment approximation) approach allowing to get the electron density of state, eDoS, and the atomic partial charges upon supplementary electron injection or upon the removal of some pristine electrons. It was found that the electron conductivity of ordered carbon nanoporous materials (calculated from the eDoS at the Fermi level in a free electron approximation) is actually lower than that of disordered nanoporous carbons and does not relate to the actual material density but rather correlates with the actual atomic arrangement in terms of percolative path of sp2 carbons atoms through out the nanotexture that is always present in disordered nanoporous (activated) carbons ; non sp2 carbons populate more the texture of carbon obtained from zeolite casting. This result holds true in a zero-charge situation as well as in charged (polarized) conditions (|0.3|e/C-atom).

In her TB simulations of an ordered porous carbon-based supercapacitor (of a 1:1 electrolyte with no explicit solvent, Cs+Cl- referred to here as the ionic fluid), Delfour proceeded in several steps: (i) the TB partial atomic charged calculated for the polarized system with no electrolyte were frozen and used in a NVT Monte-Carlo simulation of the ionic fluid adsorbing and (partially) invading the pore space from the outside external space in-between the two zeolite-replicated carbon electrodes (ii) the eDoS and the partial charges were then recalculated. Having the ions invading the pore systems did locally change the carbon atoms partial charges, typically at the vicinity of the external surface. A self-consistency scheme was used to periodically update the atomic partial charges and obtain a charge distribution consistent with the modification of the potential achieved through the modification of atomic levels. The method used to achieve self-consistence calculates the electronic structure eDoS of the whole system (carbon and ions) after MC equilibration. This involves performing a complete TB calculation, which is computationally extremely heavy and also requires the introduction of new Slater parameters to characterize the atomic levels and jump integrals associated with all species. The proximity of the ions will modify the charge distribution of the carbon atoms, and in return their own charge, requiring the above outlined self-coherent treatment. Such procedure allows the conservation of the charge of the ions and the update of the charge on the carbon atoms. (iii) a new MC simulation was then be restarted with the updated charges, and so on... until the distribution at the start and at the end of the simulation are identical (hence achieving self-consistence). Delfour's work showed that the amount of docked ions in electrodes nanopores did not change much upon this self-consistent scheme i.e the amount on ions docked in both electrodes at the first step remains almost constant. It was also shown that the eDoS remains essentially the same when comparing that of the system with its pores loaded with ions to the one calculated for the polarized system with no ionic liquid. However, the electronic conductivity (in the free electron approximation) did show a noticeable increase with a larger number of states at the Fermi level due to presence of ions. Applying the same computational scheme to disordered porous carbons (with smaller pores compared to zeolite templated carbons), Delfour did show that only the nanopores in close connection with the external surface were actually occupied by ions with a penetration depth of typically 1 nm.

The present work builds upon these theoretical results obtained from quantum methods that take electrons explicitly and uses the departure from the perfect sp2 carbon state to locate (topological and chemical) defects and attribute them a charge excess or deficit of charge depending on the polarization. Therefore, we modified the constant charge method: the electrostatic field generated by the matrix defects (here non sp2-carbon atoms and edge hydrogen species) will drive ion adsorption on the electrode external surface as well as in its nanopore. This is a key improvement with regard to the standard constant charge (CC) approach that gives all substrate atoms the same charge. It is also an improvement with respect to the constant voltage (CV) approach that assumes a perfectly conducting substrate hence accumulating/depleting charges only on the atoms at the pore and external surfaces with no regards to the intrinsically defective nature of porous carbons as electrode material. As carbon atoms at the external or pore surface are necessary defective according to our approach, they will localize charge excess/deficit. In this sense our approach is consistent with the CV approach. The neglect of substrate charge adjustment upon ion docking somewhat inclines our method to predicting to be more accurate toward the first instant of ions docking although Delfour's TB calculation show rather insignificant change in ions docking through the charge regulation process. Our approach also allows locating charges excess/deficit in the electrode core that is makes it also consistent with the standard CC method. In

sum, our computational scheme to describe a supercapacitor in functioning conditions implements the advantages of both CC and CV traditional scheme while enabling (i) the ion docking in sub nanopores (as shown by experimental evidence) and (ii) without excess adsorption of ions leading to unphysical situations where all ions of giving sign localize at the middle of the oppositely polarized electrode (see Fig. S 2).

1. Methods

The simulations has been done in a box of 52x52x105 $Å^3$ using periodic boundary conditions has been used. The temperature has been controlled using a Nose-Hoover thermostat set at 300K with a temperature damping parameter of 100fs.

A voltage has been applied to the system in order to simulate the adsorption of ions inside the electrodes. Several methods has been used to apply the charge differential on the two electrodes. First, we have used the constant voltage (CV) method developed for metallic surfaces(16–18), which has been recently recommended for studying EDL supercapacitors(19). In this method, the charges are attributed to electrode atoms and are recalculated along the dynamics. This method has been widely used to study EDL with electrolytic solution(19) and metallic systems(20). Secondly, we have used the constant charge (CC) method which consists in adding a small positive or a negative charge ΔE to all atoms of each electrode. This method is cheaper but is generally considered less reliable. However, it has been shown that it can be useful for sub-nanometer space(21) Amongst the main drawbacks of the constant charge method is that it does not adapt the charges locally when the electrolytes are adsorbed. Finally, we have used a new method that we have developed that is called chemically driven charge localization (CDCL) in which we distribute the charges according to the presence of defects in the system.

Recently, it has been shown that when imposing a voltage by imposing constant charges in the electrodes could lead to unrealistic increase in the temperature(19). To our eyes, this is a major issue that has to be tested. We have simulated a trajectory in the NVE ensemble in order to sample the evolution of the temperature over time using the constant charge method. After an equilibration of the model 1 during 50 ps at 300K in the NVT ensemble, the temperature has been recorded during a run in the NVE ensemble. In a recent work, Merlet et al. (19) observed an abnormal temperature increase using the CC scheme. Note that after analysing the trajectory, we did not observe any significant increase in the temperature (see Figure). The main differences between our systems and the system studied in Merlet et al. (19) is that we have simulated a water-based solution and that we have not placed the electrodes at the edge of the box. The increase in temperature that was observed in the literature is most likely due to a macroscopic field that has not been cancelled out.

We would like to draw the attention on the fact that the constant potential method, in our simulations, the charge density was high at the edges of the electrodes (see Fig. 4(a)), a result that did not depend on the Gaussian width parameter. In comparison to the constant charge method, there is an important difference in term of charge distribution. We have found that due to these different schemes, the ions are not adsorbed on the same sites. In the case of constant potential method, we only have ions adsorbed on the surface or in the skin of the electrodes, where the charges are large, whereas in the other method ions are adsorbed all along the profile of the electrodes (including inside pores). In the literature, the constant potential method has been shown to be able to adsorb ions inside carbon electrodes(22). However, the pore size distribution being different than ours, this is most likely adsorption in large pores(23). In pores of about 1-2 nm, the pore walls will be densely charged in the constant potential method as it is for the surface of the electrodes that will attract ions inside the electrodes (24).

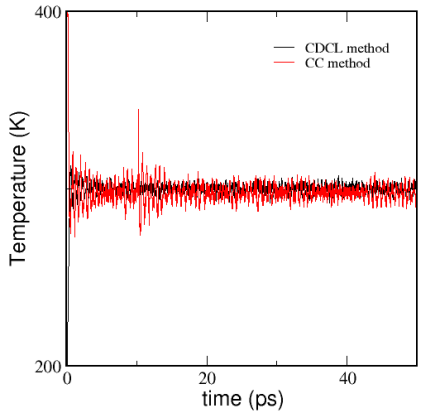

Fig. S 1. Evolution of the temperature over time showing no drift using the CC scheme and the CDCL scheme using $delta_q$ = 0.02

In our carbon-based systems, the charge should not be delocalized as it is in metals. Recently, Deschamps et al. (25) has shown experimentally that ions are being adsorbed inside the nanopores in nanoporous materials. A result that could not be reproduced by the constant voltage method, because of the charge distribution favoring adsorption on at the skin of the electrodes. Thus, the charge distribution given by the constant potential method is not realistic. The drop in the charge excess is about 0.2 e/atom if we compare the charges of carbon atoms at the surface of the electrode and in the middle. Also, in a large centered region, the charges are almost null, which leads to a majority of carbon atoms not interacting with the ions of the system. The same results were obtained applying the constant charge method only on the carbon atoms belonging to the skin of the electrode.

As observed in the literature(19), we have noted that in the constant charge method the dynamics of ions was quicker than the constant potential method. The former method does not add any computation time since the charges are fixed. Thus, the computational cost of the constant charge method is significantly reduced compared to constant potential method. However, in the constant charge simulations, the ions are being adsorbed to the center of the electrodes Fig. 4(b), and no ions remain at the surface.

In order to estimate the energy variation due to the adsorption of ions in the pore network, we have calculated the differential of energy between the initial configuration (with no adsorption) and the same configuration having one ion adsorbed in the electrode. The energy of the adsorption is about 0.083 eV, which is small compared to the bond energy

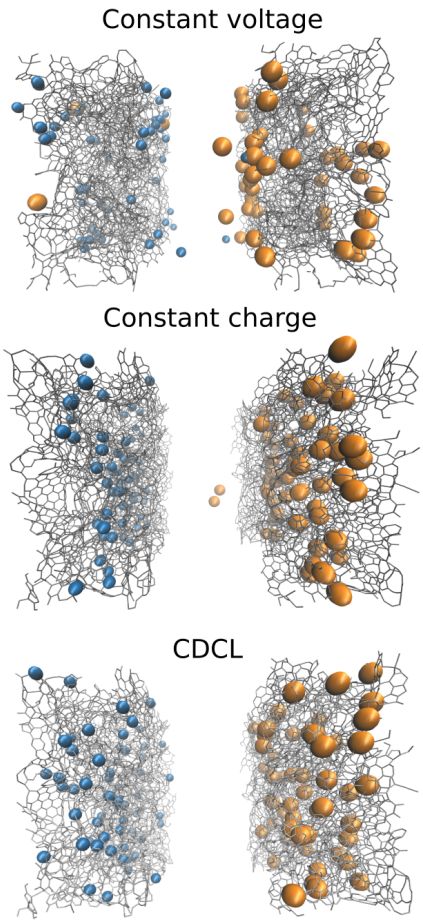

Fig. S 2. Snapshots of adsorption sites at the highest polarization. Carbon atom of around the ions are colored in orange and the aromatic rings are colored depending on their number of members. In the constant voltage method, ions are adsorbed only at the surface of the electrodes (top). In the constant charge method, ions are adsorbed both inside only deeply inside the electrode (center). In the CDCL method, the ions are adsorbed inside and on the external surface of the electrodes.

of the bonds of the system. Therefore, the presence of ions in the electrodes should have a weak influence on the charge localisation. Moreover, if the ions are adsorbed with the hydration shell the ion charge should be screened by the water molecules.

We have found that in the constant potential method, which adapts the charges locally as the ions are adsorbed, the charge variation of a carbon atom is negligible compared to a system in which no ions are adsorbed. In fact, in these supercapacitors, we do not have chemical reactions during the charge. Therefore, the presence of nearby ions should not completely change the charge distribution of atoms in the electrode.

In the chemistry driven charge localisation scheme (CDCL), the charges are attributed depending on the number of members in the aromatic ring and depending on the angle made with a carbon atom and its nearest neighbors Fig. 3. More explicitly, we attribute an additional charge (positive for the anode and negative for the cathode) to atoms making an angle far from the ideal angle for sp2 carbon (about 120°). A smoothing has been used to attribute a smaller charge the closer we are to the ideal angle.

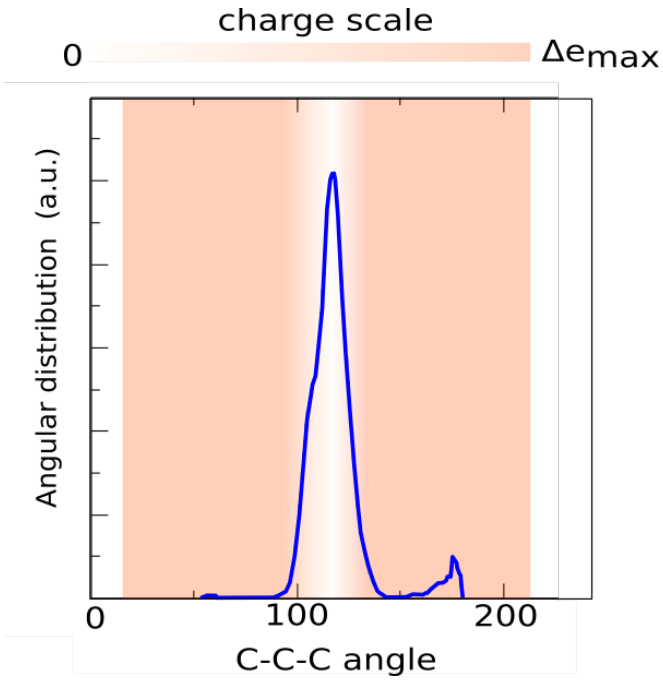

Fig. S 3. Angular distribution function of the C-C-C angles.

A. Charge distribution in the constant voltage method. The charge distribution in the constant voltage method shows that only the carbon atoms at the edge of the electrodes are charged (Fig. 4(a)). This explains why in the trajectories, we observe that the ions are adsorbed only at the external surface of the electrodes (Fig. S 2). Moreover, we have observed that the presence of ions at the surface (Fig. 4(b)) does not significantly modify the attributed charge to the carbon atom.

B. Radial distribution function. The radial distribution functions for C-O, C-Cl and C-Na show that ions and water molecules can be adsorbed in small pores of a minimum size of about 5nm. Before applying the electric field, we have observed that water molecules have entered the pore network but ions remains on the outside of the electrodes. The carbon material has a hydrophobic nature, which is reflected by the first C-water peak being localised at about 3.1Å . Ions in this system are adsorbed at a closer distance to the edges of the pores (about 2.1 Å). Therefore, ions will tend to lose their hydration shell before entering into smaller pores.

C. Capacitance. The specific capacitance has been calculated as following: $C_s = Q/(m * U)$ where Q(C) is the total charge adsorbed in the electrodes, U(V) is the voltage and m(g) is the mass of the electrodes.

D. Number of ions adsorbed in the constant charge method. Unexpectedly, we have noticed that in the constant charge method if the charges are uniformly distributed, it is necessary to apply a larger charge to the carbon atoms than in the case of a heterogeneous distribution. This result is certainly linked to how the ions are escaping their hydration shell. This is in agreement with the results discussed in the main text, in

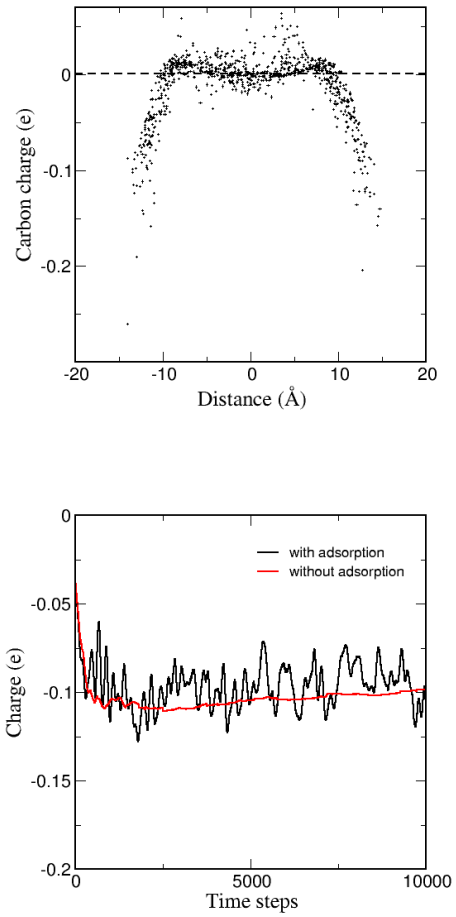

Fig. S 4. (a) Charge attributed to carbon atoms for a constant voltage of 10V depending on their position relative to the center of the electrode. The electrode is 30 Å wide, in 2/3 of the electrodes the attributed charge is close to zero. The average value is -0.01 e. (b) Evolution of charge attributed to a carbon atom on the surface of the anode during the simulation (with adsorption in black and without adsorption in red). The adsorption of ions does not modify the average value of the charge but induces small fluctuations around it.

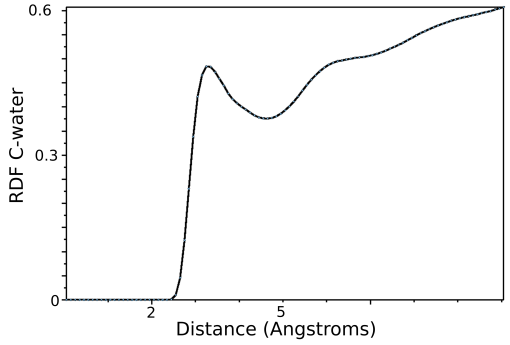

Fig. S 5. Radial distribution function for the C-O_w after absorption.

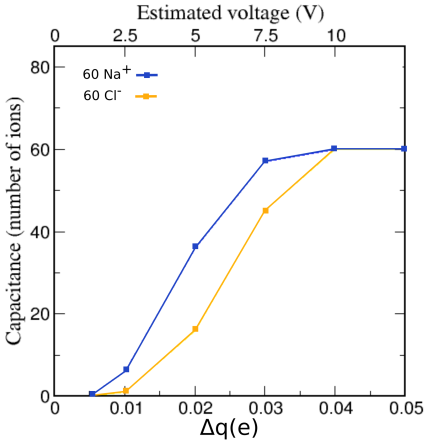

Fig. S 6. Number of ions adsorbed in the constant charge method (homogeneous distribution).

particular with the fact that we do not observe adsorption of ions inside the electrodes when we use the constant potential method, in which all the surface of the electrodes is charged and does not force the ions to leave their hydration shell.

Ions that are being adsorbed in the constant charge method (with a uniform distribution) are diffusing to the center of the electrodes Fig. 4(b) and have a fast dynamics compared to the two other methods presented in the manuscript.

To compute this energy we compared the total energy, after a minimization, between the initial system and the system after adsorption. This corresponds to the energy of adsorption for a system at constant mass. In the case of adsorbing a single ion in the constant charge method using a non-uniform distribution of additional charges, we have calculated that the energy of adsorption is only 8kJ/mol (0.083 eV).

Moreover, we have calculated the energy of adsorption in the constant charge method (with a uniform charge distribution). Fig. S 8 illustrates this energy for each simulation at different voltage. We notice that the second system with ionic fluid has a linear energy storage function of the number of adsorbed ions. Note that, we also performed simulations with different distances between the electrodes and did not notice evolution for both, capacitance and stored energy. This corresponds to a uniform and constant charge method. In this method, the adsorption energy is much higher than in the non-uniform distribution case. This is due to the fact that the constant charge method can lead to unrealistic results in which all ions are adsorbed close the the center of the electrode and therefore in more constrained pores, as mentioned previously.

E. Adsorption video (attached separately). The video shows the adsorption of chloride and sodium ions (orange and blue spheres respectively) in the electrodes. In the beginning, the full simulation box is shown, composed by the two carbon electrodes, water, chloride and sodium ions. The electrodes are colored based on the local carbon charges based on the CDCL method. For visualization reason, we depict the high charge (0.02 e) in red, low charge (between 0 and 0.02 e) in green and no charge in gray. The first part of the video zooms into the positive electrode and shows the dynamics of chloride desolvation and adsorption. The water molecules are blurred out for easier visualization of the ions and carbon network. The second part zooms into the negative electrode and shows

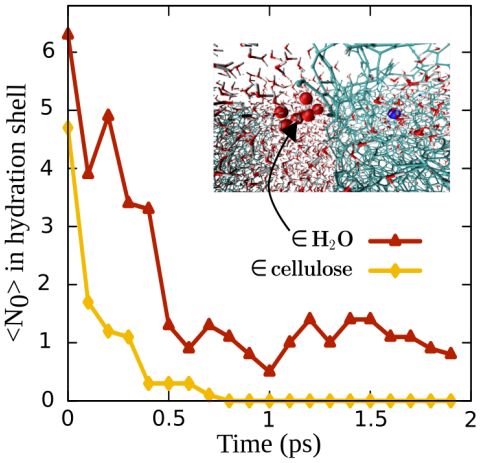

Fig. S 7. Number of oxygen in the solvation shell of sodium ions during the adsorption at Δ_e=0.02 e in the constant charge method. The snapshot represents a sodium ion after adsorption inside the electrode. This sodium ion was originally surrounded only by H2O. C, Na, O, H are represented in light blue, dark blue, red, white, respectively. Oxygen of the initial solvation shell before adsorption are represented bigger.

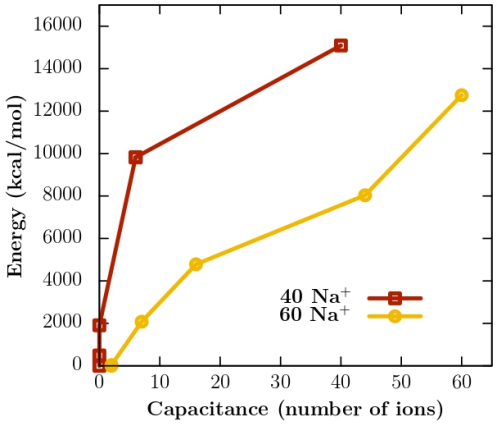

Fig. S 8. Relative energy due to the adsorption of ions for different voltage. These energies are computed after an energy minimization of the final configuration of MD runs. Squares represent simulations with only the sodium ions compensating the fiber charge. Circles represent simulations with 20 sodium and 20 chloride additional ions.

the dynamics of sodium desolvation and adsorption. The video correspond to a maximum charge $\Delta_q = 0.02$ e.

F. Lammps input file (attached separately). Input files containing the atomic structure (with different charges) and the LAMMPS script files for the adsorption simulation can be downloaded. The required files for the run are Dataset S1.txt (lammps control file), Dataset S2.txt (atomic structure file), Dataset S3.txt (lammps parameters file) and Dataset S4.txt (COMPASS parameters file). Dataset S5.txt (0V), Dataset S6.txt (0.5V), Dataset S7.txt (1V) can be used as replacement of the file Dataset S2.txt to modify the applied voltage.

G. Charge distribution in defective carbon structures. Charge distribution has been calculated on a defective activated carbon at the HF/6-31G* level using Gaussian09 and the charge analysis has been performed using the restrained electrostatic potentials scheme using Multiwfn(26). The charge distribution indicates that the charges are localised on defects and sp2 carbon atoms have a very low charge (< 0.05 q).

id	element	x	y	z	q
1	C	4.299796	-4.142917	5.229243	-0.0743127
2	C	6.643128	-4.507595	0.526798	-0.154622
3	C	-2.138801	1.618836	1.239787	0.0832421
4	C	-1.156318	-2.683266	4.772633	-0.0817598
5	C	4.466240	0.641500	-1.492439	0.00621236
6	C	-6.074999	0.860151	-1.634895	0.0109579
7	C	-1.708458	-2.131140	3.722047	0.042429
8	C	4.718697	4.867323	1.221724	0.140688
9	C	-3.903971	-0.565541	-1.126613	0.0663379
10	C	4.340655	-1.628168	-0.433674	0.316721
11	C	-3.417630	0.693617	0.939497	0.121225
12	C	-3.503384	6.756493	-0.999810	0.0287224
13	C	0.059000	7.387177	1.551828	-0.0736012
14	C	9.062146	1.255448	-3.389133	-0.0441805
15	C	-0.686608	-2.822746	-1.287651	0.0052174
16	C	6.218504	5.235974	-0.466860	0.0113979
17	C	-4.249559	0.419542	-0.231850	-0.142877
18	C	-3.646302	-0.436461	1.860371	-0.0959815
19	C	4.079919	-4.970856	3.110892	-0.170907
20	C	-1.712135	-1.879359	-1.874777	-0.0255749
21	C	-6.048993	-1.980522	-1.013763	0.0372031
22	C	-7.992005	-1.380297	3.652047	-0.146297
23	C	1.097220	8.022259	0.895975	-0.0508669
24	C	0.997259	1.617743	-2.502079	-0.196213
25	C	-6.950734	-1.344416	-0.155139	0.17816
26	C	8.085739	-0.440580	-1.675528	-0.00652712
27	C	9.695403	4.887264	-0.162271	-0.123841
28	C	-1.440578	-3.977302	-0.753018	-0.0363523
29	C	-1.525337	-5.951948	-2.418746	-0.0239381
30	C	0.057371	1.521886	2.451191	0.129477
31	C	5.062166	-3.181706	1.647777	-0.0736554
32	C	-4.391850	6.494176	-2.026559	0.126242
33	C	4.130478	1.456966	2.106477	0.0760914
34	C	4.148338	-0.117541	-0.251240	-0.116566
35	C	-2.326984	5.634014	1.051764	-0.0794096
36	C	-4.136257	3.236131	0.722688	-0.13654
37	C	3.217382	-2.461365	-0.537835	-0.159619
38	C	-6.100571	2.183251	0.122091	0.0745146
39	C	3.111593	6.605725	1.679294	0.0309416
40	C	2.499745	7.748212	1.200111	0.0266974
41	C	4.342713	-0.022347	2.511263	-0.0535251
42	C	-4.670346	3.971781	-2.635701	0.0579006
43	C	5.944665	-0.519428	-2.842303	0.114737
44	C	4.092316	4.064479	2.157458	-0.0971924
45	C	4.103751	0.345255	0.971744	-0.0151488
46	C	-4.998553	-1.292341	-1.762089	0.0143643
47	C	-7.050875	-0.846137	2.798558	0.149541
48	C	3.066023	0.006491	-5.060953	0.0115977
49	C	5.867074	0.456705	-1.865780	0.131868
50	C	-2.654959	-3.609480	0.002695	0.112145
51	C	-4.859774	7.501496	-3.026476	-0.0134399
52	C	-2.106517	-7.624336	-4.495607	-0.10299
53	C	-4.625228	5.234030	-2.291968	-0.118649
54	C	2.679131	-0.120800	-6.304778	-0.0801337
55	C	3.831995	-0.030140	-3.876258	0.293193
56	C	5.025557	-2.030727	4.021270	-0.0174916
57	C	9.698641	2.083309	-2.489970	0.00117905
58	C	-2.734271	-2.102789	0.315946	0.0846659
59	C	4.959683	-3.128999	4.730025	0.0588835
60	C	4.106933	2.757787	2.232992	0.0152415
61	C	-7.438442	0.589146	-1.812567	-0.111321
62	C	0.672385	1.232407	3.654464	-0.209144
63	C	5.088965	-0.808403	-3.890428	-0.258298
64	C	-2.324772	-2.325880	-3.132911	0.109445
65	C	5.526777	-6.687059	1.296833	-0.0483828
66	C	9.081629	2.383159	-1.250510	-0.0935886
67	C	-6.143908	-3.416923	-1.011516	0.0244227
68	C	3.093597	-4.114578	3.555494	0.195528
69	C	-2.047970	0.523390	6.064492	0.0727877
70	C	-2.828291	-3.776247	-3.085233	0.134207
71	C	-4.772343	-0.828766	5.549429	-0.0712529
72	C	-5.022267	1.607703	-2.315115	-0.0792141
73	C	-0.241222	2.027047	-2.602819	0.192181
74	C	-1.518711	2.119316	-2.872809	-0.162665
75	C	-8.330337	-1.669544	-0.335980	-0.109918
76	C	-1.177188	-5.283220	-1.259003	-0.00114732
77	C	-0.890012	1.664337	1.560270	-0.085172
78	C	1.414043	-3.285093	5.011952	-0.0319324
79	C	4.695266	-0.947133	3.367467	0.0117983
80	C	0.729641	-2.839025	-1.202602	-0.00856987
81	C	-5.710241	0.723243	-0.141270	0.249559
82	C	-2.080827	-6.535093	-3.772460	0.185049
83	C	-3.609754	2.125947	1.644991	0.158431
84	C	-0.871155	1.265614	5.804389	-0.0640832
85	C	1.987964	-2.787074	-0.846168	0.0184603
86	C	6.505695	-2.476425	-1.690434	0.0920447
87	C	7.263531	0.730019	-1.352165	-0.0963569
88	C	9.529633	3.563543	-0.611918	0.134593
89	C	-7.409134	2.543143	0.363181	-0.108174
90	C	-3.912798	1.186921	-3.121179	0.0412204
91	C	5.651123	-2.271642	-0.575928	-0.141064
92	C	-8.532747	0.689642	-0.852805	0.0125411
93	C	-4.878341	2.947386	-1.739687	0.0233455
94	C	-4.866280	-4.062428	-1.352235	0.128883
95	C	-8.451131	1.875664	-0.063218	0.0903469
96	C	-2.917754	6.184365	0.021453	0.079102
97	C	-4.549294	-2.100811	-2.889953	0.0205207
98	C	2.405904	-3.182039	4.163982	-0.0298084
99	C	-4.169430	2.099937	3.110423	-0.14635
100	C	0.124642	0.959499	4.893674	0.142095
101	C	-4.340257	0.371648	5.014155	-0.0465912
102	C	10.453926	-1.278142	-0.816509	-0.149762
103	C	-4.251447	-3.522717	-2.569890	-0.124633
104	C	-6.087296	-0.430199	2.016331	-0.301949
105	C	-2.801945	2.064937	-3.124616	0.0491832
106	C	5.865412	-5.318502	1.479592	0.108025
107	C	-3.886856	-4.345677	-0.305211	-0.125872
108	C	-2.497190	-2.401241	2.627384	-0.00817607
109	C	-7.469095	-3.863496	-0.754141	-0.042391
110	C	-2.337553	-5.012731	-3.433464	-0.141651
111	C	-2.947914	-1.595095	1.606269	-0.111044
112	C	5.421697	4.442383	0.202722	0.0109142
113	C	-6.407463	-0.336943	0.622496	-0.11953
114	C	9.356249	-0.678881	-1.202961	0.112722
115	C	5.031499	-4.435857	2.230845	0.111989
116	C	-2.640698	-1.292756	-0.902790	-0.0721224
117	C	-5.075791	3.008613	-0.292985	0.0498788
118	C	3.478807	0.625656	-2.607320	-0.267032
119	C	-3.431285	-1.459799	-3.581607	-0.0751306
120	C	5.915332	-3.222579	0.463328	0.186074
121	C	2.222855	1.168125	-2.415439	0.168807
122	C	7.204593	-1.388635	-2.538526	-0.104613
123	C	-3.562083	-0.086156	-3.604489	-0.0102249
124	C	-4.808715	-0.162154	2.607965	0.27436
125	C	4.490403	6.237291	1.376340	-0.105723
126	C	-4.637568	0.853346	3.652874	0.0627006
127	C	7.987912	1.821331	-0.801666	0.0949649
128	H	3.511407	4.607634	2.910980	0.0609416
129	H	8.200201	0.699544	-3.057960	0.0696294
130	H	7.500484	2.286295	0.056670	-0.00503805
131	H	-3.596405	4.178446	0.763532	0.0328366
132	H	4.480421	-2.297579	1.900626	-0.0245686
133	H	1.760213	1.210065	3.618653	0.0917681
134	H	-4.567178	3.698871	-3.686475	0.0204738
135	H	5.395429	3.379210	-0.050171	0.0250834

H. Desorption. After 1 ns of unloading (starting from a configuration obtained after loading the electrodes with Δ_q=0.01e (0.5V), ions are kept inside the electrode. We observe that the number of Cl^- ions trapped in the system is bigger than the number of Na^+.

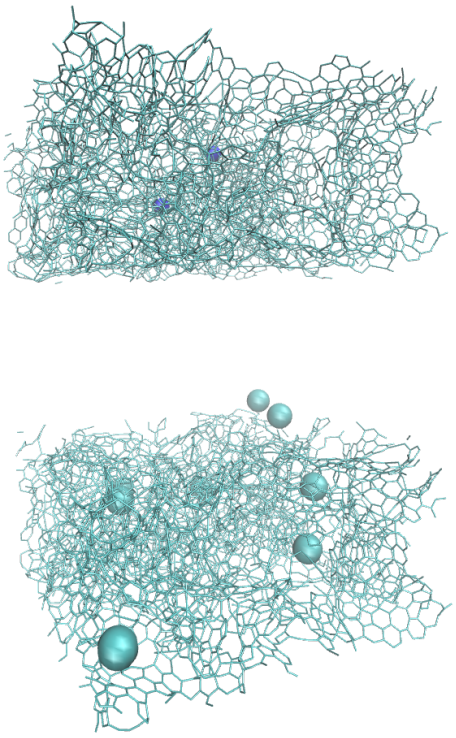

Fig. S 9. Snapshot showing Na^+ and Cl^- ions that are being trapped in the porous structure after 1 ns of unloading. For clarity, only ions at a distance less than 3 Å to the carbon atoms are shown.

1. J Pikunic, et al., Structural modeling of porous carbons: Constrained reverse monte carlo method. *Langmuir* **19**, 8565–8582 (2003).
2. A Obliger, FJ Ulm, R Pellenq, Impact of nanoporosity on hydrocarbon transport in shales' organic matter. *Nano Lett.* **18**, 832–837 (2018) PMID: 29337576.
3. D Ibrahim Abouelamaiem, et al., New insights into the electrochemical behaviour of porous carbon electrodes for supercapacitors. *J. Energy Storage* **19**, 337–347 (2018).
4. BA Mei, O Munteshari, J Lau, B Dunn, L Pilon, Physical interpretations of nyquist plots for edlc electrodes and devices. *The J. Phys. Chem. C* **122**, 194–206 (2018).
5. ME Suss, et al., Impedance-based study of capacitive porous carbon electrodes with hierarchical and bimodal porosity. *J. Power Sources* **241**, 266–273 (2013).
6. F Béguin, V Presser, A Balducci, E Frackowiak, Carbons and electrolytes for advanced supercapacitors. *Adv. Mater.* **26**, 2219–2251 (2014).
7. J Chmiola, et al., Anomalous increase in carbon capacitance at pore sizes less than 1 nanometer. *Science* **313**, 1760–1763 (2006).
8. J Segalini, B Daffos, P Taberna, Y Gogotsi, P Simon, Qualitative electrochemical impedance spectroscopy study of ion transport into sub-nanometer carbon pores in electrochemical double layer capacitor electrodes. *Electrochimica Acta* **55**, 7489–7494 (2010).
9. SA Evlashin, et al., Role of nitrogen and oxygen in capacitance formation of carbon nanowalls. *The J. Phys. Chem. Lett.* **11**, 4859–4865 (2020) PMID: 32515198.
10. G Hartmann, GS Hwang, First-principles description of electrocatalytic characteristics of graphene-like materials. *The J. Chem. Phys.* **153**, 214704 (2020).
11. T Hussain, E Olsson, K Alhameedi, Q Cai, A Karton, Functionalized two-dimensional nanoporous graphene as efficient global anode materials for li-, na-, k-, mg-, and ca-ion batteries. *The J. Phys. Chem. C* **124**, 9734–9745 (2020).
12. A Maslechko, T Verstraelen, TS van Erp, E Riccardi, Multiscale partial charge estimation on graphene for neutral, doped and charged flakes. *Phys. Chem. Chem. Phys.* **20**, 20678–20687 (2018).
13. T Roussel, et al., Experimental and atomistic simulation study of the structural and adsorption properties of faujasite zeolite-templated nanostructured carbon materials. *The J. Phys. Chem. C* **111**, 15863–15876 (2007).
14. L Delfour, *Thesis - Simulation d'un supercondensateur à l'échelle atomique.* (2011).
15. C Bichara, et al., Structure and properties of nanoscale materials: theory and atomistic computer simulation. *Int. J. Nanotechnol.* **9**, 576–604 (2012).
16. Z Wang, Y Yang, DL Olmsted, M Asta, BB Laird, Evaluation of the constant potential method in simulating electric double-layer capacitors. *The J. Chem. Phys.* **141**, 184102 (2014).
17. SK Reed, PA Madden, A Papadopoulos, Electrochemical charge transfer at a metallic electrode: A simulation study. *The J. Chem. Phys.* **128**, 124701 (2008).
18. TR Gingrich, M Wilson, On the ewald summation of gaussian charges for the simulation of metallic surfaces. *Chem. Phys. Lett.* **500**, 178 – 183 (2010).
19. C Merlet, et al., Simulating supercapacitors: Can we model electrodes as constant charge surfaces? *The J. Phys. Chem. Lett.* **4**, 264–268 (2013) PMID: 26283432.
20. SK Reed, OJ Lanning, PA Madden, Electrochemical interface between an ionic liquid and a model metallic electrode. *The J. Chem. Phys.* **126**, 084704 (2007).
21. J Yang, et al., Reliability of constant charge method for molecular dynamics simulations on edlcs in nanometer and sub-nanometer spaces. *ChemElectroChem* **4**, 2486–2493 (2017).
22. M Simoncelli, et al., Blue energy and desalination with nanoporous carbon electrodes: Capacitance from molecular simulations to continuous models. *Phys. Rev. X* **8**, 021024 (2018).
23. N Ganfoud, et al., Effect of the carbon microporous structure on the capacitance of aqueous supercapacitors. *Energy Storage Mater.* **21**, 190 – 195 (2019).
24. M Salanne, et al., Efficient storage mechanisms for building better supercapacitors. *Nat. Energy* **1**, 16070 (2016).
25. M Deschamps, et al., Exploring electrolyte organization in supercapacitor electrodes with solid-state NMR. *Nat. Mater.* **12**, 351–358 (2013).
26. T Lu, F Chen, Multiwfn: A multifunctional wavefunction analyzer. *J. Comput. Chem.* **33**, 580–592 (2012).